

# Improving Wind-Ramp Forecasts in the Stable Boundary Layer

David E. Jahn<sup>1</sup> · Eugene S. Takle<sup>1</sup> ·  
William A. Gallus Jr.<sup>1</sup>

Received: 8 April 2016 / Accepted: 17 January 2017 / Published online: 8 February 2017  
© Springer Science+Business Media Dordrecht 2017

**Abstract** The viability of wind-energy generation is dependent on highly accurate numerical wind forecasts, which are impeded by inaccuracies in model representation of boundary-layer processes. This study revisits the basic theory of the Mellor, Yamada, Nakanishi, and Niino (MYNN) planetary boundary-layer parametrization scheme, focusing on the onset of wind-ramp events related to nocturnal low-level jets. Modifications to the MYNN scheme include: (1) calculation of new closure parameters that determine the relative effects of turbulent energy production, dissipation, and redistribution; (2) enhanced mixing in the stable boundary layer when the mean wind speed exceeds a specified threshold; (3) explicit accounting of turbulent potential energy in the energy budget. A mesoscale model is used to generate short-term (24 h) wind forecasts for a set of 15 cases from both the U.S.A. and Germany. Results show that the new set of closure parameters provides a marked forecast improvement only when used in conjunction with the new mixing length formulation and only for cases that are originally under- or over-forecast (10 of the 15 cases). For these cases, the mean absolute error (MAE) of wind forecasts at turbine-hub height is reduced on average by 17%. A reduction in MAE values on average by 26% is realized for these same cases when accounting for the turbulent potential energy together with the new mixing length. This last method results in an average reduction by at least 13% in MAE values across all 15 cases.

**Keywords** Boundary-layer parametrization · Wind forecasts · Wind ramps

## 1 Introduction

In an effort to reduce the negative environmental effects of traditional power generation, such as from coal and other fossil fuels, there has been a strong interest in renewable energy, including wind energy. Since the wind speed is highly variable, accurate wind forecasts at

---

✉ David E. Jahn  
djahn@iastate.edu

<sup>1</sup> Iowa State University, 1130 Coover Hall, Ames, IA 50011, USA

turbine-hub height are crucial for the viability of wind energy as a source of electricity. Here, we propose an approach for improving mesoscale-model short-term wind forecasts (24 h) at the turbine-hub height and, in particular, accounting for wind-ramp events, which are defined as large fluctuations in wind speed over a relatively short period of time.

There is no one uniformly accepted definition of a wind ramp (Bianco et al. 2016). Certain studies use the criterion of a 50% change in wind generation relative to the total power capacity within a period of 4 h or less (Greaves et al. 2009; Deppe et al. 2013). According to the power curve of a 1.5-MW turbine (General Electric Company 2005), such a rate of change in power may be associated with a change in wind speed of  $3 \text{ m s}^{-1}$  or greater over the same time period.

There is much room for improvement in wind-ramp forecasts, and for wind forecasts at the turbine-hub height in general. The Mid-continent Independent System Operator (MISO) has shown (Navid et al. 2011) that in their region a wind-generation day-ahead forecast error exists of 8–10% of wind-generation capacity, representing up to 30% of actual wind generation. Greaves et al. (2009) found from a 15-month study that commercially available day-ahead forecasts had an accuracy of 30% in predicting wind-ramp events for selected U.S. sites and 35% for U.K. sites. For a study at a wind-farm site in Iowa, Deppe et al. (2013) found that mesoscale simulations correctly predicted little more than half of wind-ramp occurrences.

There is a consensus in the modelling community that an improved wind-speed forecast using mesoscale models requires modifications to the planetary boundary-layer (PBL) parametrization schemes. For example, see the Department of Energy workshop report on wind-resource characterization (Schreck and Lundquist 2008) and various individual studies that have analyzed mesoscale-model accuracy based on various PBL schemes (Storm and Basu 2010; Grisogono 2010; Fernando and Weil 2010; Hu et al. 2013; Deppe et al. 2013). In general, these studies found that PBL schemes inadequately represent certain dynamics associated with wind ramps in a stable boundary layer (SBL), such as the evolution of the low-level jet (LLJ) and the nocturnal cooling of the atmosphere.

While such an intercomparison and analysis of different PBL parametrization schemes are useful, little work has been done to modify and improve the performance of existing schemes beyond the work of the original authors. The exception is Olson and Brown (2012), who modified the diagnosis of turbulent-eddy scale factors (e.g. turbulent mixing length) within a given PBL scheme. Their work has resulted in considerable improvement for upper-level winds in National Weather Service operational wind-speed forecasts as well as improvement in near-surface wind-speed forecasts (Olson and Brown 2011, 2012). Their focus in making improvements to PBL parametrizations that perform well across all weather regimes and scenarios is broad and thus improvements very difficult.

The specific purpose of the current study is to improve model performance of wind ramps, which is a specific weather phenomenon associated with the nocturnal SBL. Wind ramps are often poorly forecast with substantial negative impacts to the wind-energy industry. Focusing on the improvement in wind-ramp forecasting here could enable similar studies of other weather phenomena, and thus approach the goal of a robust parametrization scheme applicable to many weather scenarios.

As stated above, the PBL scheme influences model performance especially for the stable environment. Thus, the focus here is to revisit the formulation of the Mellor, Yamada, Nakanishi, and Niino (MYNN) PBL scheme (Mellor 1973; Mellor and Yamada 1974, 1982, hereafter referred to as M73, MY74, and MY82, respectively) and to propose modifications that allow for improved forecasts of wind ramps. The MYNN scheme has been chosen because it is a widely used option for both operational models of the U.S. National Weather Service (Benjamin et al., 2013) and within the wider research community.

Three approaches are undertaken to modify this scheme to improve wind-ramp forecasts: (1) solve for a new set of closure parameters; (2) reformulate the means for calculating the turbulent mixing length; (3) allow for the explicit accounting of turbulent potential energy (TPE) in the energy budget. Closure parameters are pre-defined constants used to define an approximated linear interdependence of covariance turbulence variables, such as the momentum and heat fluxes. These approximations serve as the means of closing the system of second-order turbulence equations. [Jahn et al. \(2015\)](#) demonstrated the potential for improving numerical wind forecasts by modifying these closure parameters in the MYNN scheme.

Improving the MYNN scheme by modifying the mixing length and accounting for TPE stems from [Sun et al. \(2012 hereafter Sun12\)](#) and [Zilitinkevich et al. \(2007 hereafter ZL07\)](#) who show that Monin-Obhukov similarity theory actually fails under specific stable conditions. Updated approaches presented in Sun12 and ZL07 for the mixing-length and energy-budget calculations, respectively, are implemented as part of the PBL scheme and for improving wind-ramp forecasts.

The fundamental basis for, and dynamic influence of, closure parameters, the mixing length, and TPE are investigated in [Sect. 2](#) along with an approach for modifying their representation of boundary-layer processes. [Section 3](#) describes the set-up of a suite of wind-ramp cases and the production of numerical forecasts using the Weather Research Forecast (WRF) model ([Skamarock et al. 2008](#)). [Section 4](#) presents an analysis of the results showing a marked improvement in wind-speed forecasts, while [Sect. 5](#) provides a summary with concluding remarks.

## 2 MYNN Basic Theory and Means for Modification

### 2.1 Fundamental Theory of MYNN Scheme

The underlying theory of the MYNN scheme is based on the fundamental equations of conservation of mass and momentum. The presentation below follows closely that given by M73, MY74, and MY82. The continuity equation, equation of motion for mean velocity,  $U_j$ , and conservation of mean potential temperature,  $\Theta$ , are

$$\frac{\partial U_k}{\partial x_k} = 0, \tag{1}$$

$$\frac{\partial U_j}{\partial t} + \frac{\partial}{\partial x_k} (U_k U_j + \overline{u_k u_j}) + \epsilon_{jkl} f_k U_l \tag{2}$$

$$= -\frac{1}{\rho} \frac{\partial P}{\partial x_j} - g \delta_{j3} \beta \Theta + \nu \nabla^2 u_j, \tag{3}$$

and

$$\frac{\partial \Theta}{\partial t} + \frac{\partial}{\partial x_k} (U_k \Theta + \overline{u_k \theta}) = \alpha \nabla^2 \Theta, \tag{4}$$

for which Einstein summation notation has been adopted. Here,  $P$  is the mean pressure, while  $u_j$ ,  $\theta$ , and  $p$  are fluctuations about the mean values of wind speed, potential temperature and pressure, respectively. Reynolds-averaged values are denoted with an overbar. Also,  $g$  represents the acceleration due to gravity,  $f$  is the Coriolis parameter, and  $\beta$  is the coefficient of thermal expansion ( $\beta = -(\partial\rho/\partial T)/\rho$ ), while  $\nu$  represents the kinematic viscosity and  $\alpha$  is the kinematic heat conductivity.

In order to obtain a closed solution for these set of equations, it is necessary to obtain values for the momentum, heat flux and variance terms  $\overline{u_i u_j}$ ,  $\overline{u_i \theta}$ , and  $\overline{\theta^2}$  that represent 10 combinations of variables. The governing equations for these variables are detailed in M73, MY74, and MY82 as well as Nakanishi (2001 hereafter denoted as N01) and given here

$$\begin{aligned} & \frac{\partial \overline{u_i u_j}}{\partial t} + \frac{\partial (U_k \overline{u_i u_j})}{\partial x_k} + \overline{u_k u_i} \frac{\partial U_j}{\partial x_k} + \overline{u_k u_j} \frac{\partial U_i}{\partial x_k} \\ & = E_{distr} + E_{disp} + E_{diff} + B + F, \end{aligned} \tag{5}$$

where  $E_{distr}$  is the energy distribution term,  $E_{disp}$  is energy dissipation,  $E_{diff}$  is energy diffusion,  $B$  is buoyancy, and  $F$  is the Coriolis term; and,

$$\begin{aligned} & \frac{\partial \overline{u_j \theta}}{\partial t} + \frac{\partial (U_k \overline{\theta u_j})}{\partial x_k} + \overline{u_j u_k} \frac{\partial \Theta}{\partial x_k} + \overline{\theta u_k} \frac{\partial U_j}{\partial x_k} \\ & = H_{distr} + H_{disp} + H_{diff} + B, \end{aligned} \tag{6}$$

such that  $H_{distr}$ ,  $H_{disp}$ , and  $H_{diff}$  denote energy distribution, dissipation, and diffusion terms. Also

$$\frac{\partial \overline{\theta^2}}{\partial t} + \frac{\partial (U_k \overline{\theta^2})}{\partial x_k} + 2\overline{u_k \theta} \frac{\partial \Theta}{\partial x_k} = T_{disp} + T_{diff}, \tag{7}$$

such that terms on the r.h.s represent energy dissipation and diffusion, respectively.

This system consists of 10 differential equations that are simplified as detailed in M73, MY74, MY82 and N01, such as the boundary-layer approximation, assuming isotropy, and neglecting the time-tendency, advection, and diffusion terms. As such, the parametrization in its present form is not necessarily well posed for the SBL, in which turbulent eddies exhibit an anisotropic structure.

The simplified set of equations is

$$\overline{u^2} = \frac{q^2}{3} + \frac{A_1 L}{q} \left\{ -4\overline{uw} \frac{\partial U}{\partial z} + 2\overline{vw} \frac{\partial V}{\partial z} - 2\beta g \overline{w\theta} + 2C_2 \beta g \overline{w\theta} \right\}, \tag{8}$$

$$\overline{v^2} = \frac{q^2}{3} + \frac{A_1 L}{q} \left\{ 2\overline{uw} \frac{\partial U}{\partial z} - 4\overline{vw} \frac{\partial V}{\partial z} - 2\beta g \overline{w\theta} + 2C_2 \beta g \overline{w\theta} \right\}, \tag{9}$$

$$\overline{w^2} = \frac{q^2}{3} + \frac{A_1 L}{q} \left\{ 2\overline{uw} \frac{\partial U}{\partial z} + 2\overline{vw} \frac{\partial V}{\partial z} + 4\beta g \overline{w\theta} - 4C_2 \beta g \overline{w\theta} \right\}, \tag{10}$$

$$\overline{uv} = \frac{3A_1 L}{q} \left\{ -\overline{uw} \frac{\partial V}{\partial z} - \overline{vw} \frac{\partial U}{\partial z} \right\}, \tag{11}$$

$$\overline{uw} = \frac{3A_1 L}{q} \left\{ -\overline{w^2} \frac{\partial U}{\partial z} + \beta g \overline{u\theta} + C_1 q^2 \frac{\partial U}{\partial z} \right\}, \tag{12}$$

$$\overline{vw} = \frac{3A_1 L}{q} \left\{ -\overline{w^2} \frac{\partial V}{\partial z} + \beta g \overline{v\theta} + C_1 q^2 \frac{\partial V}{\partial z} \right\}, \tag{13}$$

$$\overline{u\theta} = -\frac{3LA_2}{q} \left[ \overline{uw} \frac{\partial \Theta}{\partial z} + \overline{w\theta} \frac{\partial U}{\partial z} (1 - C_5) \right], \tag{14}$$

$$\overline{v\theta} = -\frac{3LA_2}{q} \left[ \overline{vw} \frac{\partial \Theta}{\partial z} + \overline{w\theta} \frac{\partial V}{\partial z} (1 - C_5) \right], \tag{15}$$

and

$$\overline{w\theta} = -\frac{3LA_2}{q} \left[ \overline{w^2} \frac{\partial \Theta}{\partial z} + \overline{w\theta} \frac{\partial w}{\partial z} + g\beta \overline{\theta^2} \right] - C_3 g \beta \overline{\theta^2} + \overline{w\theta} \frac{\partial w}{\partial z} (C_4 - C_5). \tag{16}$$

Here,  $L$  represents a turbulent master length scale associated with the anticipated eddy size and thus greatly influences the effects of mixing in the boundary layer. Also,  $q$  is related to turbulent kinetic energy (TKE) such that  $q^2 = \overline{u^2} + \overline{v^2} + \overline{w^2}$ .

The full system of equations for the MYNN scheme consists also of prognostic equations for  $q^2$ ,

$$\frac{D(q^2/2)}{Dt} - \frac{\partial}{\partial z}[LqS_q \frac{\partial(q^2/2)}{\partial z}] = -\overline{uw} \frac{\partial U}{\partial z} - \overline{vw} \frac{\partial V}{\partial z} + \beta g \overline{w\theta} - \frac{q^3}{B_1 L}, \tag{17}$$

and for  $\overline{\theta^2}$ ,

$$\frac{D\overline{\theta^2}}{Dt} - \frac{\partial}{\partial z}[LqS_\theta \frac{\partial\overline{\theta^2}}{\partial z}] = -2\overline{w\theta} \frac{\partial\Theta}{\partial z} - \frac{2q}{B_2 L} \overline{\theta^2}. \tag{18}$$

Here,  $S_q$  and  $S_\theta$  are dimensionless parameters of their respective diffusion terms. Note that the above equations include a set of closure parameters ( $A_1, A_2, B_1, B_2, C_1, C_2, C_3, C_5$ ) that act as weighting functions for their associated terms and serve to define the degree of interdependence among turbulent covariance variables (e.g.,  $\overline{uw}$  or  $\overline{w\theta}$ ), TKE ( $q^2/2$ ), and the mean flow variables (e.g.,  $\partial U/\partial z$  or  $\partial\Theta/\partial z$ ).

### 2.2 Formulation of New Closure Parameters

Here we calculate a new set of closure parameters appropriate for the numerical forecasting of wind-ramp events. The first step is to manipulate Eqs. 8 through 16 to obtain expressions for each closure parameter. To ensure application of the results to the full boundary layer and not just to the surface layer, explicit expressions for the closure parameters are derived without invoking certain relationships among atmospheric variables that are applicable only for the surface layer as done in N01.

Although a suite of expressions are derived for all eight closure parameters, numerical simulations of wind ramps as part of a previous study demonstrated the most sensitivity to  $A_1, B_1$ , and  $C_1$  (Jahn et al. 2015), where

$$A_1 = \frac{\frac{q}{3L} \overline{uv}}{-\overline{uw} \frac{\partial U}{\partial z} - \overline{vw} \frac{\partial V}{\partial z}}, \tag{19}$$

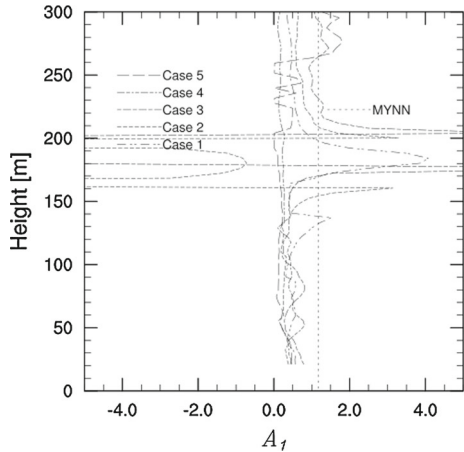
$$B_1 = \frac{q^3/L}{\overline{uw} \frac{\partial U}{\partial z} + \overline{vw} \frac{\partial V}{\partial z} - g\beta \overline{w\theta}}, \tag{20}$$

and

$$C_1 = \frac{\overline{w^2}(\frac{\partial U}{\partial z} + \frac{\partial V}{\partial z}) - \beta g(\overline{u\theta} + \overline{v\theta}) + C_2\beta g(\overline{u\theta} + \overline{v\theta}) + \frac{q}{3A_1 L}(\overline{uw} + \overline{vw})}{q^2(\frac{\partial U}{\partial z} + \frac{\partial V}{\partial z})}. \tag{21}$$

Explicit values for the turbulent flux variables on the r.h.s. are obtained using a large-eddy simulation (LES) model, based on initial conditions as provided from a tall tower near Hamburg, Germany for five cases randomly selected from a larger domain of cases that fit the following criteria: (1) There was a change in wind speed at 110m of at least 3 m s<sup>-1</sup> over a 1-h period or less; (2) The wind ramp was not the result of a frontal passage or nearby convection; (3) The airflow at a height of 110 m had an easterly component (to alleviate the impact of the city of Hamburg to the north-west of the tall tower).

**Fig. 1** Vertical profile of calculated  $A_1$  for all five Hamburg wind-ramp cases. The vertical line marks the original MYNN value,  $A_1 = 1.18$



Specifically, the WRF-LES model (Yamaguchi and Feingold 2012) is used. The model domain is three-dimensional, but the initial state is assumed horizontally uniform and thus can be initialized using one-dimensional soundings of mean wind speed and potential temperature for each case. These soundings are extracted from mesoscale-model forecasts of the five wind-ramp cases at a time shortly after the set-up of a wind ramp using the MYNN scheme in its original form. (The mesoscale-model set-up is described in Sect. 3). The LES model is run at a 4-m resolution both horizontally and vertically with a domain size of  $65 \times 65 \times 200$  points, consistent with that used by N01. (Preliminary tests with a domain of  $100 \times 100 \times 200$  points yielded similar results).

All LES simulations are initialized over 2 h, the time period required to establish a stable solution as indicated by a horizontally-averaged TKE vertical profile exhibiting relatively small variation over the last simulation hour. The mean state of the domain is kept quasi-constant during the simulation by nudging the mean velocity and potential temperature profiles back to their initial state every 5–10 min. Constant latent and sensible heat fluxes, obtained from the same mesoscale forecasts as the initial soundings, are imposed at the surface throughout the simulation. The model invokes periodic boundary conditions in the horizontal directions. The turbulent fluxes produced by the LES model were validated by verifying that the model TKE values and profiles were consistent with TKE derived from tall-tower observations, respectively, for the five cases.

The three-dimensional fields of turbulent variables are horizontally averaged to provide a vertical profile of turbulent fluxes to calculate profiles for all closure parameters based on Eqs. 19 through 21 and expressions for the remaining closure parameters (not shown). Results for  $A_1$  are given in Fig. 1.

It is worth noting that in the region of maximum wind speed at and above the LLJ (above approximately 150 m), the variance, covariance, and wind shear are *all* relatively small and approach zero (Eq. 19), falling below the anemometer range of error ( $\pm 0.02 \text{ m}^2 \text{ s}^{-2}$ ) (Bruemmer et al. 2012). Data fidelity at this scale is questionable and the physical interdependence of these terms in Eq. 19 is not necessarily valid. As a result, the values for  $A_1$  at and above the LLJ vary considerably with height.

Of primary interest, however, is the value of  $A_1$  within the boundary layer below the LLJ. Here,  $A_1$  converges to a narrow range of values for all five cases. Note that in the centre of the boundary layer (approximately 100 m height), certain terms in Eq. 19 tend toward zero

**Table 1** The original and new MYNN closure parameters

|          | $A_1$ | $A_2$ | $B_1$ | $B_2$ | $C_1$ | $C_2$ | $C_3$ | $C_5$ |
|----------|-------|-------|-------|-------|-------|-------|-------|-------|
| Original | 1.18  | 0.67  | 24.0  | 15.0  | 0.14  | 0.73  | 0.34  | 0.20  |
| New      | 0.38  | 0.61  | 15.0  | 11.4  | 0.03  | 0.73  | 0.79  | 0.20  |

in the denominator (e.g.  $\partial V/\partial z$  and  $\overline{vw}$ ), while related terms in the numerator (e.g.  $\overline{uv}$ ) also tend to be very small. In such a situation, it is appropriate to apply L'Hopital's rule to avert a singularity and achieve a well-behaved solution as shown in Fig. 1. Values for  $A_1$  are averaged vertically in the centre of the boundary layer as well as across all five cases. The result is  $A_1 = 0.38$ , which is roughly one-third the  $A_1$  value in the original closure parameter set of the MYNN scheme.

In the same manner, turbulent-flux variables obtained from the LES data are used to calculate the full set of closure parameters based on Eqs. 20 and 21 and other similar expressions for  $A_2, B_2, C_2, C_3,$  and  $C_5$  (Table 1). The application of these new closure parameter values in the MYNN scheme is denoted as method B.

### 2.3 Formulation of New Mixing Length

While MY82 emphasize the importance of closure parameters (or “closure constants” in their work), they leave the possibility that modifying the turbulent mixing length ( $L$  in Eqs. 8 to 16) could also affect PBL scheme performance because of the strong influence that mixing has on boundary-layer stratification.

In the MYNN scheme, the mixing length is diagnosed as

$$\frac{1}{L} = \frac{1}{L_S} + \frac{1}{L_T} + \frac{1}{L_B}. \tag{22}$$

The first term on the r.h.s. considers stability through the Obukhov length; the second term allows for the influence of TKE above the surface; the third term accounts for the dynamic response after vertical displacement in a stable atmosphere (see N01 for details). This formulation limits vertical mixing in the case of a stable environment, consistent with Monin-Obukhov theory. However, Sun12 provide evidence that the vertical extent of turbulent mixing is more pronounced in the SBL especially for regimes with relatively high wind shear (e.g. LLJs).

Using data from the Cooperative Atmosphere-Surface Exchange Study in 1999 (CASES-99, Poulos et al. 2002), Sun12 discovered a high correlation between turbulent energy and wind speed for wind speeds above a certain threshold value, which increases with height. Situations in which the wind speed remains below the threshold, turbulence intensity and mixing length are restricted by atmospheric stability and defined by local shear. When wind speeds exceed the threshold, turbulence intensity increases with the mean wind speed. Sun12 associate turbulence intensity with a bulk shear of the boundary layer rather than being strictly defined by the local shear at a given level.

This theory of Sun12 is used as a basis here for formulating an arbitrary expression for  $L$  in stable conditions when the mean wind speed is above a given threshold,  $V_s$ , such that

$$L = 0.75z_{BL} \frac{(V(z) - V_s)}{V_{rel}}. \tag{23}$$

Here,  $z_{BL}$  is a diagnosed boundary-layer depth (height above which the stratification is neutral), and  $V_z$  is the mean wind speed at a given height. Rather than increasing  $V_s$  with

height explicitly, the ratio  $(V(z) - V_s) / V_{rel}$  and thus also the mixing length increase with the wind speeds at higher elevations. Here,  $V_{rel}$  limits the calculated mixing length to a fraction of the boundary-layer height. (The ratio on the r.h.s. of Eq. 23 is not allowed to be greater than one). Here,  $V_{rel}$  is set to  $10 \text{ m s}^{-1}$  for all experiments. Also, if the mixing length calculated from Eq. 23 is smaller than that from Eq. 22, the latter is used.

The application of Eq. 23 is presented as an initial, and admittedly rudimentary, attempt to demonstrate the effect of maintaining a level of turbulence and associated mixing in the boundary layer even under stable conditions. As discussed in Sect. 4.2, this approach, here referred to as method C, shows promising results by giving forecasts in relatively good agreement with observations for a set of wind-ramp cases.

It is important to note that Sun12 based their theory on turbulence data from towers of height not greater than 55 m. The formulation of Eq. 23 also assumes an increase in vertical mixing above a certain threshold at higher elevations in the boundary layer, even though the appropriate threshold value at a given level in the middle and upper boundary layer is not yet explicitly known. Based on a few preliminary tests, WRF-model results for method C cases (using the MYNN scheme with updated closure parameters but with a mixing length based on Eq. 23) are optimum when the threshold wind speed  $V_s = 8 \text{ m s}^{-1}$ . It should be noted that Eq. 23 is used only for the SBL, when  $\partial\theta/\partial z > 0.001 \text{ K m}^{-1}$  and  $z > z_{min}$ . This new mixing length was applied only above  $z_{min}$  in order to avoid altering the interaction of the MYNN scheme with its associated surface-layer scheme at lower levels. The value of  $z_{min}$  is set to 50 m for method C experiments.

### 2.4 Implementation of an Energy- and Flux-Budget Turbulence-Closure Model

In the development of the original MYNN scheme as described in MY74 and MY82, model equations are simplified using a scale analysis whereby terms of order  $a_{ij}^2$  are eliminated. Here,  $a_{ij}$  is a non-dimensional measure of anisotropy that defines a departure from isotropy as given in MY74 as

$$\overline{u_i u_j} = \left[ \frac{\delta_{ij}}{3} + a_{ij} \right] q^2. \tag{24}$$

Here,  $\overline{u_i u_j}$  represents the suite of turbulent momentum flux variables given in Einstein notation, and  $q^2/2$  is the TKE. While anisotropy is not entirely ignored, some caution is warranted when deploying the MYNN scheme for scenarios in which anisotropy is not negligible, such as for the SBL in which vertical motion is impeded and turbulent eddies are not isotropic (MY82).

ZL07 propose an alternative PBL scheme based on energy- and flux-budget (EFB) equations of TKE with TPE and vertical turbulent fluxes of momentum and buoyancy. ZL07 defines TPE as

$$E_p = \frac{1}{2} \left[ \frac{\beta}{N} \right]^2 \overline{\theta^2}, \tag{25}$$

where  $N$  is the Brunt-Väisälä frequency and  $\beta = g/T_0$  is a buoyancy parameter for which  $T_0$  is a reference absolute temperature. It is worth noting that, because TPE is directly dependent on the potential temperature variance,  $\overline{\theta^2}$ , the MYNN scheme implicitly also considers the effects of TPE as evidenced by its inclusion of a temperature-variance budget equation, as well as a temperature-variance term as part of the heat-flux variance equation.

What differentiates the scheme of ZL07 from MYNN, is the argument against the existence of a Richardson-number threshold that would otherwise dictate the suppression of nearly all turbulence given an environment of sufficient stability. In ZL07, TPE and associated vertically

directed energy,  $E_z$ , never reach zero even in a strongly stable environment. The expression for  $E_z$  as offered in ZL07 is given here in simplified form,

$$E_z = K_1 E_K \psi_3 + K_2 t_{diss} \beta \overline{w\theta}, \tag{26}$$

where  $K_1$  and  $K_2$  are constants and  $t_{diss} = L/E_z^{0.5}$  represents a turbulent dissipation time scale. The first term on the r.h.s. determines the exchange of TKE ( $E_K$ ) from the horizontal to the vertical direction as designated by the stability parameter  $\psi_3$ , the effect of which is determined by a flux Richardson number,  $R_{if}$ . ZL07 give an expression for  $R_{if}$  in terms of TPE,

$$R_{if} = \frac{E_P}{E_{tot}}, \tag{27}$$

such that  $E_P$  is the TPE, and  $E_{tot} = E_K + E_P$  is the total energy of the system. The second term on the r.h.s. of Eq. 26 is related to TPE, being dependent on  $\beta$  and  $\overline{w\theta}$ .

A more explicit expression for Eq. 26 is given in ZL07 based on an array of equations,

$$E_z = \left[ S_z \left( \Pi - \left( \frac{3}{C_r \psi_3} + 1 \right) \Pi R_{if} \right) L \right]^{(2/3)}, \tag{28}$$

$$S_z = \left[ \frac{C_K C_r \psi_3}{3(1 + C_r)} \right], \tag{29}$$

$$\psi_3 = 1 + C_3 R_{if}, \tag{30}$$

$$\Pi = \overline{uw} \frac{\partial U}{\partial z} + \overline{vw} \frac{\partial V}{\partial z}, \tag{31}$$

$$\overline{uw} = -2\psi_\tau E_z^{1/2} \frac{\partial U}{\partial z} L, \tag{32}$$

$$\overline{vw} = -2\psi_\tau E_z^{1/2} \frac{\partial V}{\partial z} L, \tag{33}$$

and

$$\psi_\tau = C_{\tau 1} + C_{\tau 2} R_{if}. \tag{34}$$

The constants  $C_r = 3$ ,  $C_K = 1.08$ ,  $C_{\tau 1} = 0.228$ ,  $C_{\tau 2} = -0.208$ , and  $C_3 = -2.25$  are empirically derived in ZL07.

The following expression for  $E_z$  can then be derived as such,

$$E_z = \left\{ 2S_z \psi_\tau L^2 \left[ \left( \frac{\partial U}{\partial z} \right)^2 + \left( \frac{\partial V}{\partial z} \right)^2 \right] \left( 1 - R_{if} \left( \frac{3}{C_r \psi_3} + 1 \right) \right) \right\}, \tag{35}$$

and an explicit value for  $E_z$  then allows for calculation of turbulent fluxes  $\overline{uw}$  and  $\overline{vw}$  as given in Eq. 28. Finally, an expression for  $\overline{w\theta}$  given directly in ZL07 is

$$\overline{w\theta} = - \frac{2C_F E_z^{1/2} L}{1 + 2C_\theta C_F C_K N^2 L^2 E_z^{-1}} \left( \frac{\partial \Theta}{\partial z} \right), \tag{36}$$

where the constants  $C_\theta = 0.3$  and  $C_F = 0.285$  have also been empirically defined. The vertical gradient of potential temperature is defined based on a bulk difference spanning the boundary-layer depth. The length scale,  $L$ , is calculated here in the same manner as for method C above.

For the theory of ZL07 to be implemented into the WRF model, values for eddy viscosity and conductivity are determined by

$$K_M = -\frac{\overline{uw}}{\partial U / \partial z}, \quad (37)$$

and

$$K_H = -\frac{\overline{w\theta}}{\partial \Theta / \partial z}, \quad (38)$$

and are used to effect the evolution of the remaining turbulent fluxes. This new method based on the theory in ZL07 is labelled method D.

### 3 Methodology

Modifications to the MYNN parametrization using methods A-D are tested with a set of 15 cases, which are arbitrarily selected from wind-ramp events associated with a nocturnal SBL as identified using tall-tower observations in both Germany and Iowa in the U.S.A. Wind ramps are defined here as a change in wind speed at 100 m (in the U.S.A.) or at 110 m (in Germany) of 3 m s<sup>-1</sup> or more within 2 h or less. Cases are chosen where available evidence suggested wind ramps are primarily the result of the nocturnal inertial oscillation. Thus, care is taken to exclude cases for which ramps are caused by a frontal passage or nearby convection. Also, the topography of cases in Iowa and Germany is relatively flat, which minimizes the effects of complex terrain. Details of the 15 cases are given in Jahn (2016, hereafter Jahn16) six of which are from Germany and nine from Iowa.

The Meteorological Institute of the University of Hamburg provided sonic-anemometer observations at 50, 110, and 175 m heights a.g.l. from a tall tower just south-east of Hamburg. The base data consist of the orthogonal wind components  $u$ ,  $v$ ,  $w$  with a 1% accuracy and are averaged temporally at a 1-m resolution (Bruemmer et al. 2012). The TKE is available as a derived quantity from turbulent variance data at the vertical levels mentioned above. The Iowa Energy Center provided horizontal 10-min averaged wind data,  $u$  and  $v$ , from tall towers in Iowa near Altoona and Mason City at heights 50 to 200 m a.g.l. at 50-m intervals (Truepower 2010).

The WRF model (version 3.5.1) was used to generate 24-h wind forecasts initialized on the first day of the respective case at 1200 LT (local time = UTC + 1 h for Hamburg cases and UTC - 6 h for Iowa cases). This start time generally coincided with midday heating and allowed for 6–9 h of cooling (depending on the season) towards the evening before the collapse of the convective boundary layer and the evolution of the SBL. Two one-way nested grids, centered either over Hamburg or Iowa, were used and consisted of horizontal resolutions of 12 and 4 km (Hamburg) or 10 and 3.33 km (Iowa). The Hamburg cases used an outer horizontal grid of 121 × 121 points and an inner grid of 172 × 172 points. The Iowa cases used grids of 101 × 101 and 151 × 151 for outer and inner grids, respectively. The vertical extent up to 100 hPa was depicted using a stretched grid of 46 sigma levels with the lowest 10 set at 7.8, 21.6, 37.2, 52.9, 68.6, 84.36, 104.1, 133.7, 177.2, and 250.8 m a.g.l.

The Modern-Era Retrospective Analysis for Research and Applications (MERRA) data files (Lucchesi 2012) were used for model initial and boundary conditions for the forecasts over Germany every 6 h and were obtained from the NASA Global Modeling and Assimilation Office through the Goddard Earth Sciences Data and Information Services Center. The North

American Regional Reanalysis (NARR) data (Mesinger et al. 2006) provided the initial conditions for the Iowa forecasts and boundary conditions every 3 h.

For each of the 15 cases, a 24-h forecast was generated four different times using the WRF model with the MYNN scheme formulated according to methods A–D as described above. The Noah land-surface scheme (Chen and Dudhia 2001) and the WRF single-moment 5-Class (WSM5) microphysical scheme (Hong et al. 2004) were used for all runs. The cumulus parametrization scheme of Kain–Fritsch (Kain 2004) was used only for the 12-km or 10-km grids. Shortwave radiation processes were represented by the Dudhia scheme (Dudhia 1989) and longwave radiation by the rapid radiative transfer model (RRTM) (Mlawer et al. 1997).

Because primary interest here is to assess the model accuracy in forecasting wind ramps, each forecast was evaluated against observations using the mean absolute error (MAE) averaged over a 6-h window centered at the time of the observed wind ramp. The MAE value is based on wind speeds at tall-tower levels for which observations were available near turbine-hub height (100 m for Iowa and 110 m for Hamburg).

## 4 Results

The calculated MAE values for all 15 cases are shown in Fig. 2. Three subsets, groups 1–3, are defined according to the success of the WRF-model forecast with the original closure parameters (method A), viz. the model under-forecasts, forecasts well, or over-forecasts the wind ramp at hub height. The specific criteria for each subset are given in Table 2. Figure 3 shows WRF wind-speed forecasts for methods A–D for an example case from each of the three subsets.

It should be noted that the modified PBL schemes (methods B–D) were invoked in the WRF model only if the boundary layer was sufficiently stable ( $\delta\theta/\delta z > 0.001 \text{ K m}^{-1}$  over the boundary-layer depth). As such, for cases other than those exhibiting a stably-stratified environment, model performance and the representation of turbulence fluxes are not affected.

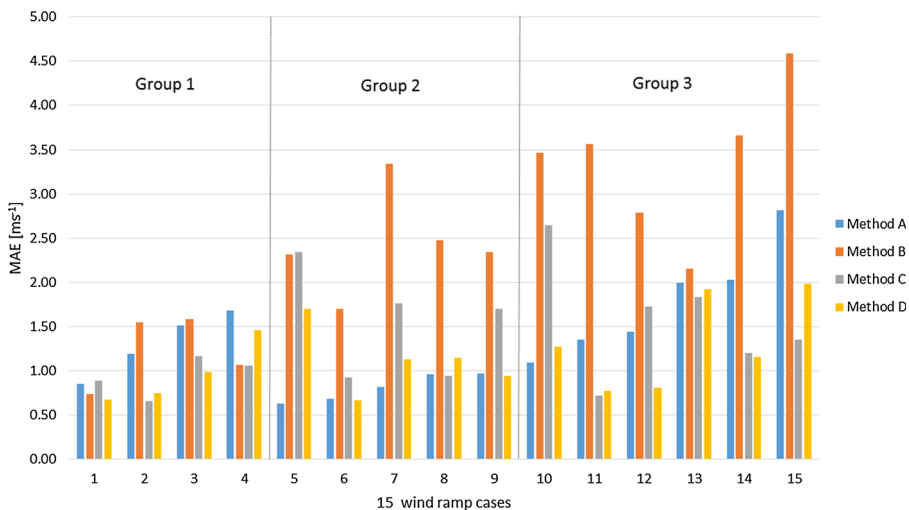


**Fig. 2** Calculated MAE for WRF-model forecasts using methods A–D for all 15 cases. The method for calculating the MAE is described in the text. Groups 1–3 denote under-forecast, well forecast, and over-forecast cases according to criteria listed in Table 2

**Table 2** Criteria for categorizing cases by subset based on *MAE* values and associated bias

| Group | Description         | Criteria  |
|-------|---------------------|---|
| 1     | Under-forecast ramp | $MAE > 0.75 \text{ m s}^{-1}$ and bias $< -0.5 \text{ m s}^{-1}$                  |
| 2     | Well forecasted     | $MAE < 1.0 \text{ m s}^{-1}$ and $\text{abs}(\text{bias}) < 0.5 \text{ m s}^{-1}$ |
| 3     | Over-forecast ramp  | $MAE > 1.0 \text{ m s}^{-1}$ and bias $> \text{zero}$                             |

Such a result is confirmed in Fig. 3 where velocity forecasts with variations in the PBL scheme are highly similar for the same case during the daytime when the boundary layer is convective (from forecast initiation at 1200 LT to roughly 1800 LT). The results of forecasts using methods B–D do not diverge until after the SBL develops after sunset. A detailed analysis of the results of these PBL scheme methods in the context of the nocturnal SBL is presented below.

#### 4.1 Method B Results and Analysis

Wind forecasts based on method B (as well as other methods) for an example case of group 1 from Hamburg on 4 September 2010 are shown in Fig. 3a. The original version of the MYNN scheme (method A) does not produce a wind ramp at 1800 LT and overall under-forecasts wind speeds during the time period of the nocturnal SBL between approximately 1800 and 0600 LT. The *MAE* value for the method A forecast is  $1.2 \text{ m s}^{-1}$ . While method B does generate a wind ramp, its forecast value is greater than the observed wind speeds, both during the wind ramp and throughout the night. The *MAE* value for method B for this case is  $1.6 \text{ m s}^{-1}$ , which is a 30% increase in *MAE* values compared with method A.

Method B consistently forecasts higher wind speeds at hub height compared with method A for all 15 cases, which improves all Group 1 results (the under-forecast cases). Although method B in the case above essentially over-corrected wind speeds resulting in an increase in forecast error, Table 3 shows an overall average decrease in *MAE* by 6% for group 1 based on method B compared with method A.

Regarding cases in groups 2 and 3 for which wind speeds are either well forecast or over-forecast using method A, the effect of method B is always to increase forecasted wind speeds more than what is observed, thus uniformly degrading forecast accuracy. The *MAE* values increase from  $0.8 \text{ m s}^{-1}$  to  $2.4 \text{ m s}^{-1}$  on average for group 2 cases (nearly a 200% increase) and increase from  $1.8 \text{ m s}^{-1}$  to  $3.4 \text{ m s}^{-1}$  for group 3 cases (an 88% increase). The *MAE* averaged across all 15 cases increases by 86%. Figures 3b, c show a marked over-forecasting of wind speeds for example cases from groups 2 and 3 using method B.

To identify why modifying the set of closure parameters according to method B always results in higher forecast wind speeds, it is necessary to examine the fundamental expressions of Eqs. 8–18 to isolate the impact of the specific terms to which any one closure parameter is associated. This is very difficult given the nonlinear nature of the systems of equations that involve terms associated with eight closure parameters. Fortunately, it is possible to limit investigation to a short list of three closure parameters,  $A_1$ ,  $B_1$ , and  $C_1$ , for which there has been found the highest degree of forecast sensitivity according to Jahn16.

The parameter  $A_1$  is associated with numerous terms, and the effect of changing its value on specific dynamic processes is difficult to isolate. However, Jahn16 found in general that decreasing  $A_1$  to half its original value results in a marked increase in forecasted wind speeds for wind-ramp cases. The parameter  $B_1$  is associated only with one term, the TKE dissipation term (Eq. 17), and its effects are more easily analyzed. Dissipation acts to reduce turbulent

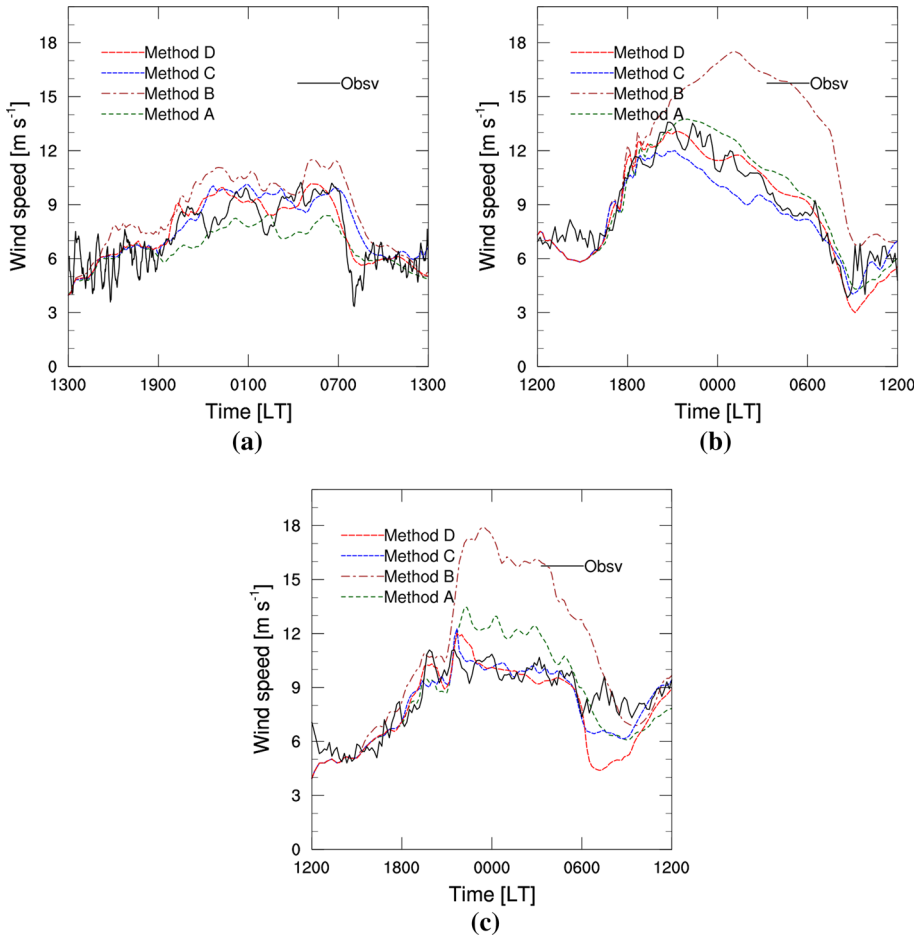


**Fig. 3** WRF-model simulated wind speeds using methods A–D (as described in the text) for **a** Hamburg case from Group 1 on 4 September 2010, **b** Altoona, IA case from group 2 on 3 October 2007, and **c** Altoona, IA case from group 3 on 12 May 2007. Forecast and observed wind speeds are given at a height of 110 m for the Hamburg case and at 100 m for the Altoona, IA cases

energy and thus also turbulent mixing that would otherwise enable the vertical transport of air parcels with relatively low momentum in the boundary layer, resulting in the reduction in LLJ strength. With  $B_1$  reduced from 24 to 15 for method B, dissipation increases, TKE and thus mixing is reduced and a stronger LLJ is allowed to develop compared with the control case (method A).

The parameter  $C_1$ , through the third term on the r.h.s. in Eq. 12, directly determines the flux,  $\overline{uw}$ . From Eq. 2, however, it is the vertical gradient of  $\overline{uw}$  that determines mean wind speed. If we consider the change in  $\partial\overline{uw}/\partial z$  only due to the change in the  $C_1$  term,

$$\Delta\left(\frac{\partial\overline{uw}}{\partial z}\right) \equiv \Delta(C_1) \frac{\partial U}{\partial z} \frac{\partial q^2}{\partial z}, \tag{39}$$

where  $\partial U/\partial z > 0$  and does not vary significantly with height at 100 m. Based on LES results of wind-ramp cases described in Sect. 2.2 and Jahn16, it is generally found that a maximum

**Table 3** MAE values [ $\text{m s}^{-1}$ ] averaged by groups

|                | Method A | Method B |             | Method C |            | Method D |              |
|----------------|----------|----------|-------------|----------|------------|----------|--------------|
|                | MAE      | MAE      | % Diff      | MAE      | % Diff     | MAE      | % Diff       |
| Avg. Group 1   | 1.31     | 1.23     | -5.8        | 0.94     | -28.0      | 0.97     | -26.2        |
| Avg. Group 2   | 0.81     | 2.43     | 198.9       | 1.53     | 88.3       | 1.12     | 37.1         |
| Avg. Group 3   | 1.79     | 3.37     | 88.3        | 1.58     | -11.6      | 1.32     | -26.2        |
| <b>Average</b> | 1.34     | 2.49     | <b>86.2</b> | 1.40     | <b>4.4</b> | 1.16     | <b>-13.3</b> |

TKE ( $q^2/2$ ) occurs in the middle of the boundary layer and often below 100 m. It is thus assumed  $\partial q^2/\partial z < 0$  at 100 m, and the r.h.s. of Eq. 39 is negative. Note that the l.h.s. is also negative. From Eq. 2, when  $\partial \overline{uw}/\partial z < 0$ , the time rate of change of wind speed increases. Thus, when  $\Delta C_1$  is reduced, the amount that wind speed would have increased is also reduced. In agreement with the results from Jahn16, the simulated wind speed at turbine-hub height during and after a wind ramp is significantly reduced when  $C_1$  is reduced to half its original value (while keeping the other closure parameters the same).

In summary, decreasing  $A_1$  and  $B_1$  individually to half their original values results in an increase in WRF-model wind speeds at hub height. Conversely, halving  $C_1$  decreases wind speeds. For the new set of closure parameters (Table 1),  $A_1$  is reduced by 68% and  $B_1$  by 38%, which if forecast sensitivity to these parameters is monotonic, would suggest an increase in WRF-model wind speeds. However,  $C_1$  is reduced significantly in the new closure parameter set, which would suggest a decrease in forecast wind speeds. The fact that the wind speeds uniformly increase for all 15 cases suggests that the combined influence of  $A_1$  and  $B_1$  on the forecast is more dominant than  $C_1$ .

## 4.2 Method C Results and Analysis

Wind forecasts improved markedly (Fig. 2) when using the new mixing length per method C as compared with method B. The average MAE value decreases from 2.5 to 1.4  $\text{m s}^{-1}$  (Table 3). The impacts on individual cases from groups 1–3 are analyzed below.

Figure 3a shows an improvement in the forecast winds for an example case of group 1 from Hamburg on 4 September 2010. Wind speeds are closer to observations for much of the 24-h forecast period for method C compared with methods A and B. From Fig. 4, it is clear that  $L$  is calculated to be larger using Eq. 23 resulting in more boundary-layer mixing especially during the wind ramp, the 4 h before midnight local time. In general, the vertical profiles of wind speeds are closer to observations for method C compared with method B (Fig. 5a). The resulting MAE value of 0.7  $\text{m s}^{-1}$  is a 44% reduction from the original MAE value of 1.2  $\text{m s}^{-1}$ . Although potential temperatures cool close to observations at lower levels (50 m) for forecasts of both methods B and C (Fig. 5b), the enhanced mixing with method C results in a deeper SBL compared with method B such that by 2300 LT, the potential temperature cools over a deeper depth for the boundary layer and corresponds to observations at both 110 and 175 m.

Other cases of group 1 (specifics not shown) similarly show wind speeds that are consistently over-forecast using method B (the WRF model with new closure parameters but using the original mixing length) are uniformly reduced with method C (WRF model with new closure parameters and new mixing length). In general, the MAE value for forecasts using method C for group 1 cases is reduced by 28% on average with respect to method A.

**Fig. 4** Time series of WRF-model forecast normalized mixing length at 110 m (Hamburg cases) or 100 m (Iowa cases) using method C for example cases from group 1 (Hamburg on 4 September 2010), group 2 (Altoona, Iowa on 3 October 2007), and group 3 (Altoona, Iowa on 12 May 2007). The mixing length for method C is normalized relative to the mixing length for method B at the same time

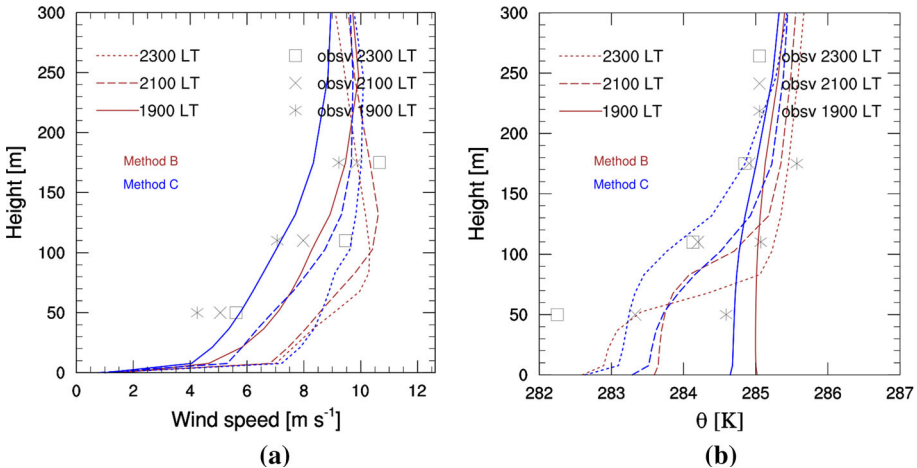
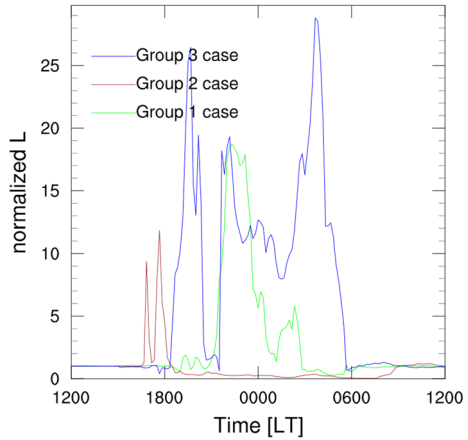


**Fig. 5** Vertical profiles of WRF-model, **a** wind speed, and **b** potential temperature at selected times using method B (brown) and method C (blue) for the Hamburg case on 4 September 2010. The initial time coincides with the wind-ramp peak. Dots represent the Hamburg tall-tower observations at commensurate times

For group 2, the average MAE value using method C is  $1.5 \text{ m s}^{-1}$ , which is 88% larger than for method A, but with a 37% reduction compared with the MAE value using method B,  $2.4 \text{ m s}^{-1}$ . This effect is seen for one case in Fig. 3b from Altoona, Iowa 3 October 2007 where wind speeds at 100 m, which are over-forecast by up to  $6 \text{ m s}^{-1}$  during the 24-h forecast with method B, are reduced considerably using method C, so much so that in this case, wind speeds are under-forecast by as much as  $6 \text{ m s}^{-1}$ . The new mixing length generates more mixing for method C as evident in the changes in vertical wind-speed profiles and potential temperature for this case (Figs. 6a, b). There is a marked cooling at levels above 50 m for method C, which suggests an increase in boundary-layer depth compared with method B, so that simulated potential temperatures approach observed values by 0100 LT. This mixing over a deeper boundary layer per method C apparently impedes the development of a strong wind-speed peak just below 100 m as seen with method B, resulting in a reduction in forecast wind speeds with method C compared with method B.

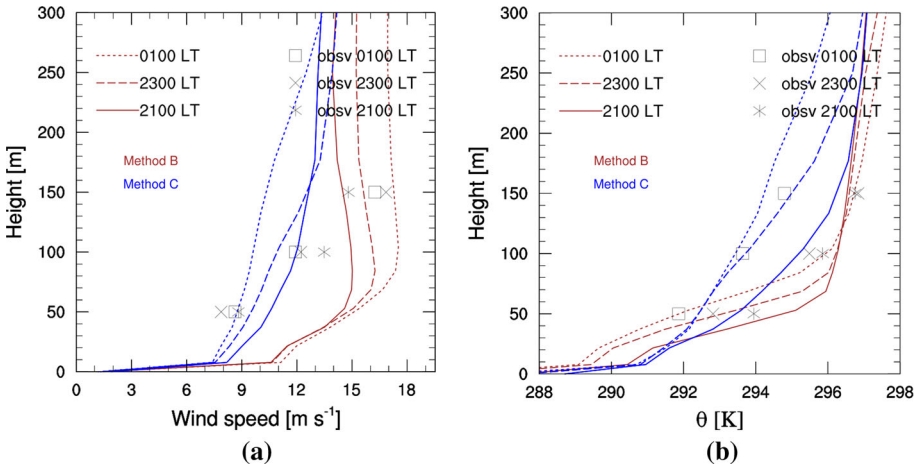


Fig. 6 As in Fig. 5, but for the Altoona, Iowa case on 3 October 2007

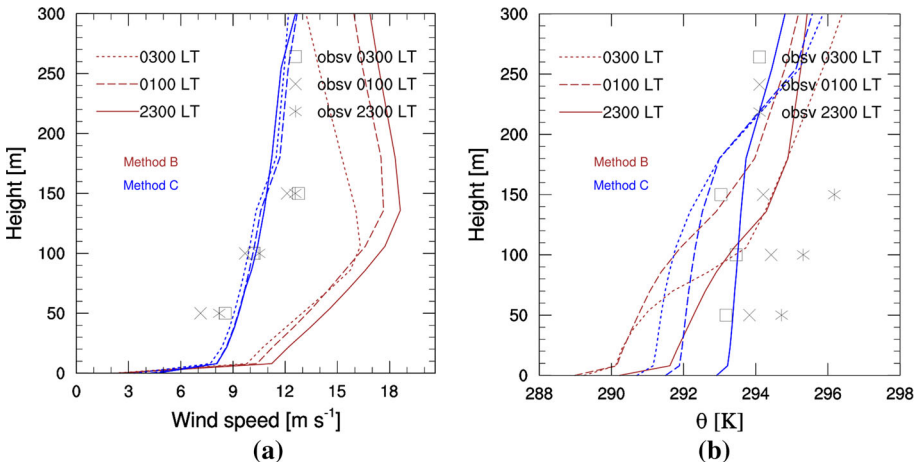
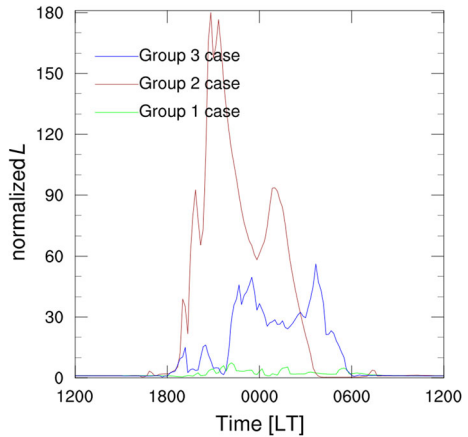


Fig. 7 As for Fig. 5, but for the Altoona, Iowa case on 12 May 2007

For Group 3 cases, the average *MAE* value for method C of  $1.6 \text{ m s}^{-1}$  is less than  $1.8 \text{ m s}^{-1}$  for method A (a 12% reduction) and much less than the average *MAE* value of  $3.4 \text{ m s}^{-1}$  for method B (a 53% reduction). For a specific case from group 3, Fig. 3c shows a wind-ramp peak at 100 m that is over-forecast by 2 to  $3 \text{ m s}^{-1}$  and 6 to  $8 \text{ m s}^{-1}$  using methods A and B, respectively. Method C, however, generates a forecast relatively close to observations. Figures 7a, b show lower temperatures over a greater depth for method C compared with method B, and the result here is a boundary layer that is generally cooler than observed. Mixing over a deeper boundary layer based on method C prevents the development of a LLJ at relatively low levels and a wind profile closer to observations compared with method B.

**Fig. 8** As for Fig. 4 for time series of mixing length calculated for method D forecasts and is normalized relative to the mixing length for method B



### 4.3 Method D Results and Analysis

Method D implements an EFB turbulence-closure model per ZL07 using the MYNN framework in the WRF model with the original closure parameter values. Both the original and new closure parameters have minimal bearing, because the calculation of turbulent fluxes in the original MYNN scheme is largely replaced by the approach in ZL07 that is mostly dependent on its own set of parameters. The mixing length is calculated in the same manner as for method C using Eq. 23. Here,  $z_{min} = 75$  m and  $V_s = 10$  m s<sup>-1</sup> for groups 1 and 2 experiments, and  $V_s = 8$  m s<sup>-1</sup> for group 3 as prescribed based on a series of preliminary tests.

Wind-speed forecasts are notably improved for method D compared with method A for group 1. On average, the *MAE* value is reduced by 26%, which is close to the reduction in *MAE* using method C (28%). Referring again to the same group 1 example case on 4 September 2010 (Fig. 3a), the overall forecast is not grossly different among methods C and D. For method D, an initial wind-ramp peak of nearly 11 m s<sup>-1</sup> is about 1 m s<sup>-1</sup> higher than observed and occurs roughly an hour earlier. An *MAE* value of 0.8 m s<sup>-1</sup> is slightly higher than 0.7 m s<sup>-1</sup> for method C, although markedly better than method A with a value of 1.1 m s<sup>-1</sup>.

A relatively large mixing length of roughly 18 times larger than method B at a height of 110 m is diagnosed for method C that persists over a 2.5-h period slightly after the initial wind ramp, around 2130 LT. Method D diagnoses a less pronounced increase in mixing length, of roughly 5 to 8 times the size of method B over the period (1800 to 0600 LT). With less mixing for method D (as diagnosed at 110 m height), the lower boundary layer cools more for method D and is closer to observations compared with method C as seen in the potential temperature profiles for 2100 and 2300 LT in Fig. 9b. A slightly cooler and lower boundary layer for method D is a consistent phenomenon among other group 1 cases.

As discussed in Sect. 2.4, a difference in the treatment of TPE among methods C and D is anticipated. Although there is a slight increase of both TKE and TPE in the boundary layer for this case (not shown), the amount is not nearly as pronounced for cases from groups 2 and 3. The effect of implementing an EFB turbulence-closure model on PBL scheme performance and in the context of an analysis of TKE and TPE will therefore be considered below for two subsequent cases.

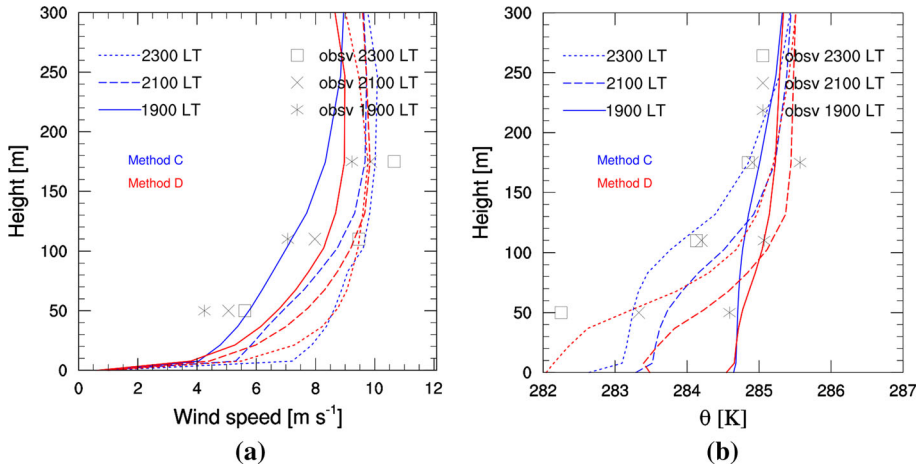


**Fig. 9** As for Fig. 5 for the Hamburg case on 4 September 2010 showing vertical profiles of forecast **a** wind speed, and **b** potential temperature using method C (blue) and method D (red)

For group 2 cases, there is evidence of improvement in method D forecasts over method C. Forecasts based on method D exhibit an average *MAE* value 37% higher than method A (see Table 3), which is better than method C forecasts with an average *MAE* value 88% higher. The example case for group 2 from Altoona, Iowa on 3 October 2007 (Fig. 3b) gives a wind-speed forecast at 100 m closer to the observations during the full forecast period compared with methods B and C. The wind speeds based on methods A and D are similar and both forecasts for this case render an *MAE* value of  $0.7 \text{ m s}^{-1}$ . It is worth noting that wind speeds based on method D at lower boundary-layer levels are over-forecast with values about  $3 \text{ m s}^{-1}$  higher than observations at the height of 50 m (Fig. 10a).

Comparing Figs. 4 and 8, the mixing length for method D is notably larger than for method C during the wind ramp. Both methods demonstrate pronounced spikes early on after the collapse of the boundary layer in the evening. Similar to group 1 cases, method D allows for more pronounced cooling compared with method C in the latter half of the forecast period in the lower boundary layer (Figs. 10b and 11b). However, just above the surface, both methods C and D forecasts show strong cooling. The difference is that for method D, cooler air is mixed to overlying levels, which does not occur with method C. Evidence of stronger mixing is consistent with pronounced TKE and TPE as is seen in Fig. 11 for method D compared with method C, especially at the time of the wind ramp around 2000 LT. Here, TPE is calculated according to Eq. 25.

Overall, method D produces wind-speed forecasts for group 3 that are significantly improved compared with the other methods. On average, the *MAE* value is  $1.3 \text{ m s}^{-1}$ , which is a 26% reduction in *MAE* value compared with method A. Figure 3c gives evidence of this trend for a previously analyzed case from 12 May 2007. Both methods C and D convincingly correct wind speeds that are largely over-forecast using method A. The mixing length for this case is roughly twice as large for method D compared with method C (Figs. 4 and 8). Likewise for Group 2, enhanced vertical mixing for method D is also consistent with larger values of TKE and TPE compared with method C, especially during the period of the initial wind ramp around 2300 LT (Fig. 13). Even with such pronounced mixing per method D for this case and the associated cooling in the lower boundary layer, the vertical profile for wind

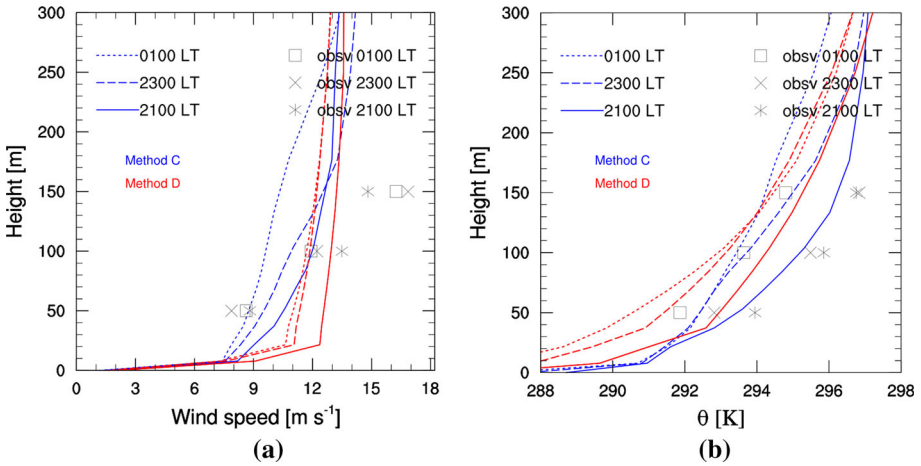


**Fig. 10** As for Fig. 9, but for the Altoona, Iowa case on 3 October 2007

speed in Fig. 12a develops similarly to what is observed using method C. This suggests that the mixing has a greater influence on the thermodynamic than on the momentum vertical transport.

### 5 Summary and Future Work

Wind ramps present a challenge to the wind-energy industry because of the relatively large change in energy production that can occur over just a few hours, making it difficult for operational planning of electricity generation. The work undertaken herein has sought to improve wind-ramp forecasts by modifying the MYNN scheme, which is a popular turbulence parametrization scheme used in the WRF model, using a three-pronged approach: (1) Formulate a new set of closure parameters for the MYNN scheme appropriate for wind-ramp events using the fundamental equations of the turbulence-closure model and sample turbulence-flux data generated by a LES model; (2) Formulate a new method for calculating the turbulent mixing length to enhance mixing in the SBL for cases of relatively large wind shear; (3) Explicit accounting of turbulent potential energy in the energy budget.

For a set of 15 wind-ramp cases from both Iowa in the U.S.A. and Hamburg, Germany, WRF-model forecasts are generated using the MYNN scheme with both the original set of closure parameters (method A) and the new set (method B). It is found that using the new closure parameters uniformly results in an increase in forecast wind speeds at a height of 100 m. Therefore, the only cases for which improvement is realized are those cases for which the original closure parameter set (method A) significantly under-forecasts wind speed to the extent that the average MAE value is reduced by 6% (group 1, Table 3). There is some indication that group 1 cases exhibit relatively light winds aloft compared with the other cases. It is possible that the evolution of the SBL for group 1 is not as greatly influenced by dynamics aloft compared with changes brought on by the set-up of the SBL at lower levels. In this sense, these cases conform more closely to the idealized model by which the inertial oscillation determines the set-up of the LLJ. However, more work is required to quantify this hypothesis.

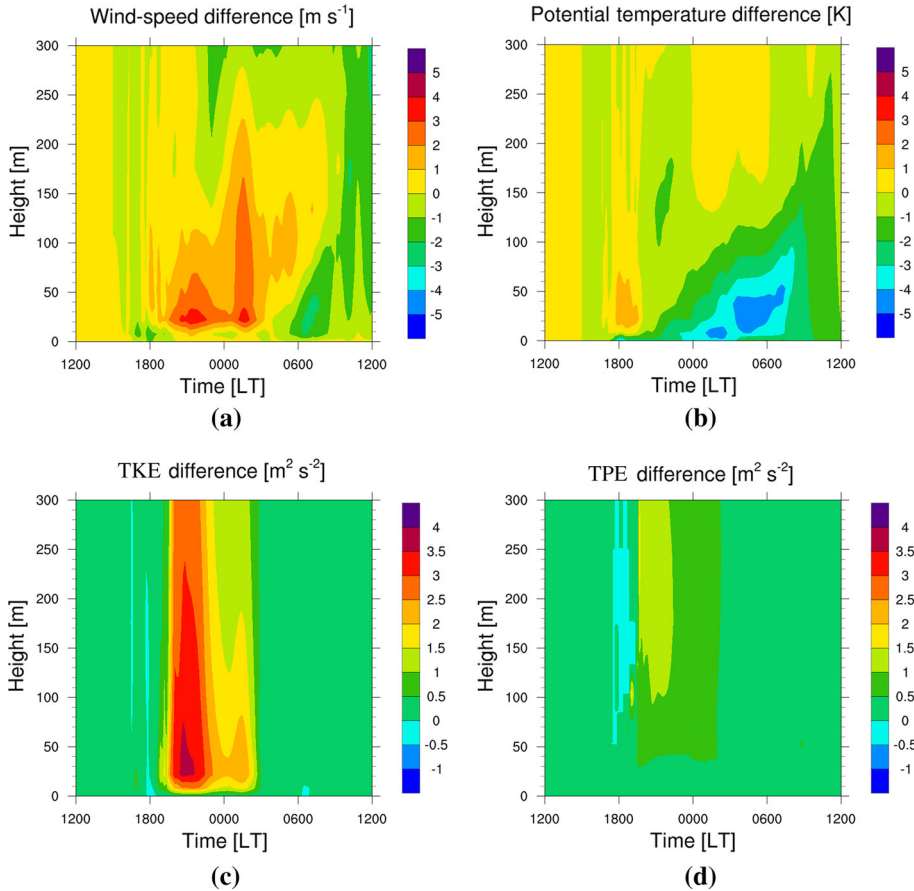


**Fig. 11** Time vs. height plots of the difference in fields of WRF-model forecasts using method D compared with method C for the same case as Fig. 10 for the Altoona, Iowa case on 3 October 2007. Differences are shown for **a** wind speed, **b** potential temperature, **c** TKE, and **d** TPE

Because only marginal improvements have been realized by using a new set of closure parameters in the MYNN scheme with no other modifications, a new method for calculating the turbulent mixing length was considered. The amount of mixing in the boundary layer greatly influences the stratification. Although according to conventional thinking stability impedes large-scale mixing, relatively new findings by Sun12 indicate the possibility of some mixing dependent on the bulk shear in stable environments for wind speeds exceeding a certain threshold. Motivated by the results of Sun12, a new approach to calculating the turbulent mixing length in the MYNN scheme has been formulated. The results have shown a uniform improvement for forecasts using both the new closure parameter set and the new mixing length (method C) compared with forecasts with the new set of closure parameters and the original formulation of mixing length (method B). There is also a marked improvement for cases that demonstrate a significant under- or over-forecast of wind speeds using the original set of closure parameters (method A). There is clear indication that including a mixing length that incorporates larger-scale mixing across the depth of the boundary layer,

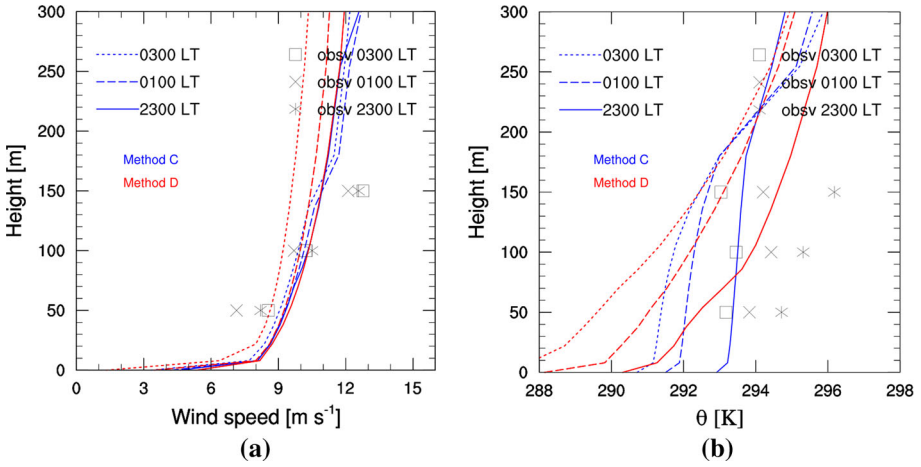


Fig. 12 As in Fig. 9, but for the Altoona, Iowa case on 12 May 2007

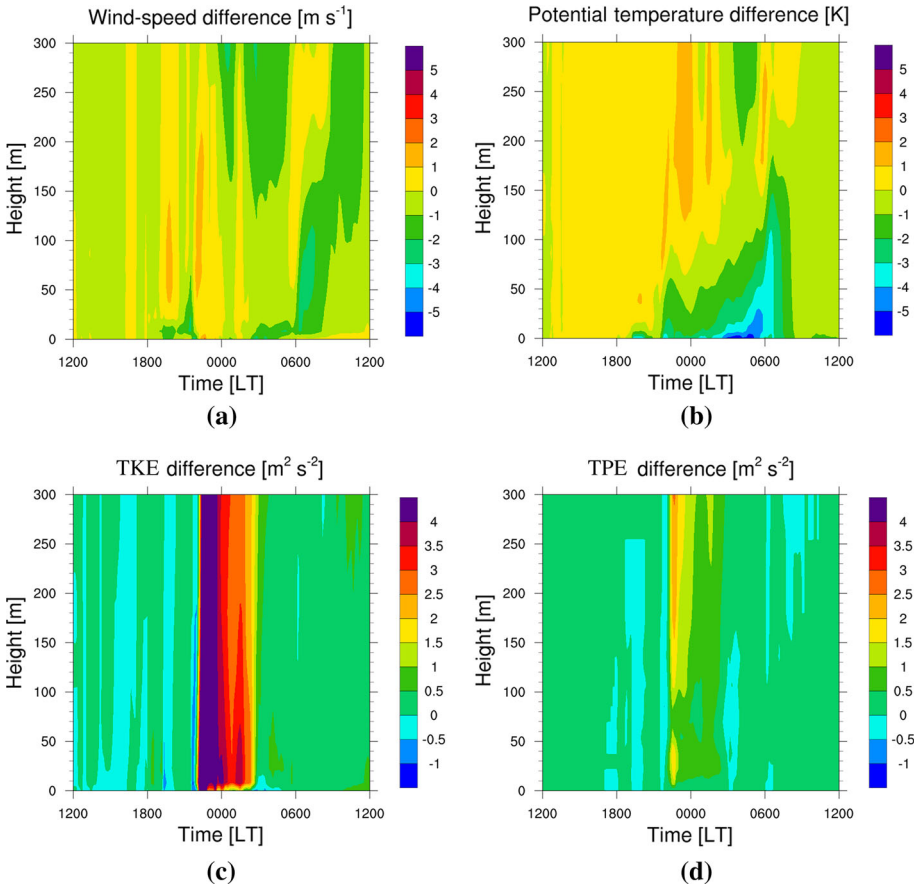


Fig. 13 As in Fig. 11, but for the Altoona, Iowa case on 12 May 2007

even under stable conditions, is important and conforms to what has been observed in the atmosphere.

To address the concern that the formulation of the original MYNN scheme does not adequately consider the role of TPE in the vertical mixing of a SBL, an alternative approach as presented by ZL07 for calculating turbulent fluxes has been incorporated into the MYNN framework of the WRF model (method D). Based on the set of cases in this study, results show nearly the same improvement with method C for the originally under-forecast wind-ramp cases using method A (a reduction in average *MAE* values of 28%) and the best performance among all methods for cases originally with over-forecast wind ramps (reduction in *MAE* values of 26%). Method D provides superior results in the WRF model compared with the MYNN scheme in its original form (method A) with an average reduction in forecast *MAE* values across all 15 cases of 13%.

A reduced forecast error of 13% can be viewed as significant when assessing its effect in terms of cost savings to wind-farm operations. In a DoE report stemming from its Atmosphere to Electrons (A2e) Initiative (U. S. Department of Energy 2014), it is stated that wind-speed forecast improvements of 10–20% can save \$100–300 million in annual operating costs nationally. This level of anticipated monetary value of wind-forecast improvement is also corroborated by a study conducted over the Electric Reliability Council of Texas domain such that only a 1% reduction in *MAE* value of 6-h wind forecasts is associated with an order of \$30 million cost savings over a 6-month period just within the Texas region (Orwig et al. 2012).

It is worthwhile to note that a 13% improvement in forecast accuracy is in consideration of the full suite of 15 test cases, which, although limited in number, are not at all homogeneous. Such a forecast improvement is thus possible without a priori knowledge of the different range of environmental effects that are a factor in wind-ramp evolution among the 15 cases. If, however, it is possible to identify wind-ramp cases for which the WRF model using the original MYNN scheme would under-forecast (group 1) or over-forecast (group 3) the wind ramp, the results in this study reveal a possible *MAE* reduction of as much as 28% as per method C for group 1 cases. This is predicated on having a better understanding of the primary environmental forcings (on small and large scales) that would differentiate wind-ramp development among groups 1, 2, and 3.

Although impacts on surface and near-surface temperature were not systematically analyzed, the temperature changes resulting from enhanced nighttime mixing under stratified conditions may influence the thermally driven processes in the surface layer. There also may be impacts for WRF-model applications to regional climate modelling through systematic changes to the surface energy budget.

**Acknowledgements** This work was supported by the U.S. National Science Foundation (NSF) through its Integrated Graduate Education and Research Traineeship (IGERT) Program, award 1069283. Partial support was provided by the NSF also under the State of Iowa EPSCoR Grant 1101284 and by funds through the Iowa State University Foundation associated with the Pioneer Hi-Bred Agronomy Professorship. Partial support was also provided by NSF grant AGS1624947. The tall-tower meteorological observations were provided through the Tall Tower Wind Measurement Project that was conducted by AWS Truepower and funded by the Iowa Energy Center and the U.S. Dept. of Energy. The tall-tower data from Germany were provided through the Hamburg Meteorological Institute associated with the University of Hamburg. The High Performance Center at Iowa State University provided the bulk of the computing resources used in this study to run WRF and WRF-LES for the suite of experiments. Appreciation is given to the reviewers, who provided very insightful and helpful comments.

## References

- Bianco L, Djalalova IV, Wilczak JM, Cline J, Calvert S, Konopleva-Akish E, Finley C, Freedman J (2016) A wind energy ramp tool and metric for measuring the skill of numerical weather prediction models. *Weather Forecast* 31:1137–1156
- Bruemmer B, Lange I, Konow H (2012) Atmospheric boundary layer measurements at the 280m high Hamburg weather mast 1995–2011: mean annual and diurnal cycles. *Meteorol Z* 21:319–335
- Chen F, Dudhia J (2001) Coupling an advanced land surface-hydrology model with the Penn State–NCAR MM5 modeling system, Part I: model implementation and sensitivity. *Mon Weather Rev* 129:569–585
- Deppe AJ, Wa Gallus, Takle ES (2013) A WRF ensemble for improved wind speed forecasts at turbine height. *Weather Forecast* 28(1):212–228. doi:[10.1175/WAF-D-11-00112.1](https://doi.org/10.1175/WAF-D-11-00112.1)
- Dudhia J (1989) Numerical study of convection observed during the winter monsoon experiment using a mesoscale two-dimensional model. *J Atmos Sci* 46:3077–3107
- Fernando HJS, Weil JC (2010) Whither the stable boundary layer? A shift in the research agenda. *Bull Am Meteor Soc* 91(11):1475–1484. doi:[10.1175/2010BAMS2770.1](https://doi.org/10.1175/2010BAMS2770.1)
- General Electric Company (2005) 1.5 MW series wind turbine. Technical report, GE Energy Report.A4, p 4
- Greaves B, Collins J, Parkes J, Tindal A, Hassan G, Vincent S, Lane S (2009) Temporal forecast uncertainty for ramp events. *Wind Eng* 33(4):309–320
- Grisogono B (2010) Generalizing z-less mixing length for stable boundary layers. *Q J R Meteorol Soc* 136(646):213–221. doi:[10.1002/qj.529](https://doi.org/10.1002/qj.529)
- Hong SY, Dudhia J, Chen SH (2004) A revised approach to ice microphysical processes for the bulk parameterization of clouds and precipitation. *Mon Weather Rev* 132:103–120
- Hu XM, Klein P, Xue M (2013) Evaluation of the updated YSU planetary boundary layer scheme within WRF for wind resource and air quality assessments. *J Geophys Res* 118:1831–1844
- Jahn DE (2016) Improvement of numerical wind forecasts at wind turbine height for wind ramp events within the stable boundary layer PhD thesis. Iowa State University, Ames
- Jahn DE, Takle ES, Gallus WA (2015) Sensitivity of numerical wind forecasts to variations in the closure constants of the MYNN boundary layer scheme in context of low-level jet cases within a stable boundary layer. In: 3rd international conference on Energy and Meteorology, Boulder, CO, 22–26 June
- Kain JS (2004) The Kain–Fritsch convective parameterization: an update. *J Appl Meteorol* 43:170–181
- Lucchesi R (2012) File specification for MERRA products. Technical report, NASA Global Modeling and Assimilation Office, no. 1 version 2.3
- Mellor G, Yamada T (1974) Hierarchy of turbulence closure models for planetary boundary layers. *J Atmos Sci* 31:1791–1806
- Mellor GL (1973) Analytic prediction of the properties of stratified planetary surface layers. *J Atmos Sci* 30:1061–1069
- Mellor GL, Yamada T (1982) Development of a turbulence closure model for geophysical fluid problems. *Rev Geophys Space Phys* 20(4):851–875
- Mesinger F, DiMego G, Kalnay E, Mitchell K, Shafran PC, Ebisuzaki W, Jović D, Woollen J, Rogers E, Berbery EH, Ek MB, Fan Y, Grumbine R, Higgins W, Li H, Lin Y, Manikin G, Parrish D, Shi W (2006) North American regional reanalysis. *Bull Am Meteor Soc* 87(3):343–360. doi:[10.1175/BAMS-87-3-343](https://doi.org/10.1175/BAMS-87-3-343)
- Mlawer EJ, Taubman SJ, Brown PD, Iacono MJ, Clough SA (1997) Radiative transfer for inhomogeneous atmospheres: RRTM a validated correlated-k model for the longwave. *J Geophys Res* 102:16663–16682
- Nakanishi M (2001) Improvement of the Mellor–Yamada turbulence closure model based on large-eddy simulation data. *Boundary-Layer Meteorol* 99:349–378
- Navid N, Rosenwald G, Chatterjee D (2011) Ramp Capability for Load Following in the MISO Markets. Technical Report 1, MISO Market Development and Analysis. <https://www.misoenergy.org/Library/Repository/CommunicationMaterial/KeyPresentationsandWhitepapers/RampCapabilityforLoadFollowinginMISOMarketsWhitePaper.pdf>
- Olson J, Brown JM (2011) Modifications in the MYNN PBL surface scheme to improve the AK coastal barrier jet and overall performance in the rapid refresh. In: Alaska weather symposium 2011 proceedings, Alaska
- Olson J, Brown JM (2012) Modifications in the MYNN PBL and surface layer schemes for WRF-ARW. In: WRF user’s workshop 2012 proceedings, Boulder, CO
- Orwig K, Hodge BM, Brinkman G, Ela E, Milligan M (2012) Economic evaluation of short-term wind power forecasts in ERCOT: preliminary results. In: 11th annual international workshop on large-scale integration of wind power into power systems as well as on transmission networks for offshore wind power plants conference, Nov 13–15. National Renewable Energy Laboratory, Lisbon

- Poulos SG, Blumen W, Fritts DC, Lunquist JK, Sun J, Burns SP, Nappo C, Banta R, Newsom R, Cuxart J, Terradellas E, Balsley B, Jensen M (2002) CASES-99: a comprehensive investigation of the stable nocturnal boundary layer. *Bull Am Meteorol Soc* 83:551–581
- Schreck S, Lundquist J, W S (2008) U.S Department of Energy workshop report: research needs for wind resource characterization. Technical Report NREL/TP-500-43521, National Renewable Energy Laboratory
- Skamarock WC, Klemp J, Dudhia J, Gill DO, Barker DM, Duda MG, Huang XY, Wang W, Powers JG (2008) A description of the Advanced Research WRF version 3. Technical report, National Center for Atmospheric Research, NCAR Technical Note NAR/TN-475+STR, p 113
- Storm B, Basu S (2010) The WRF model forecast-derived low-level wind shear climatology over the United States Great Plains. *Energies* 3(2):258–276. doi:10.3390/en3020258
- Sun J, Mahrt L, Banta RM, Pichugina YL (2012) Turbulence regimes and turbulence intermittency in the stable boundary layer during CASES-99. *J Atmos Sci* 69(1):338–351. doi:10.1175/JAS-D-11-082.1
- Truepower A (2010) Iowa tall tower wind assessment project. Technical report, Iowa Energy Center, final report, p 66
- U. S. Department of Energy (2014) Atmosphere to electrons (A2e) initiative overview. Tech. rep., DOE Wind and Water Power Technologies Office. <http://energy.gov/sites/prod/>
- Yamaguchi K, Feingold G (2012) Technical note: large-eddy simulation of cloudy boundary layer with the advanced research WRF model. *J Adv Model Earth Syst*. doi:10.1029/2012MS000164
- Zilitinkevich SS, Elperin T, Kleorin N, Rogachevskii I (2007) Energy- and flux-budget (EFB) turbulence closure model for stably stratified flows. Part I: steady-state, homogeneous regimes. *Boundary-Layer Meteorol* 125:167–191